Journal of Southeast University (English Edition) Vol. 23, No. 4, pp. 534 – 539 Dec. 2007 ISSN 1003—7985

Manipulation of nanoparticles by AC electrothermal effect in laboratory-on-a-chip applications

Lian Meng[1] Wu Jie[1] Jiang Hongyuan[2] Yang Hukun[2]

([1]Department of Electrical Engineering and Computer Science, The University of Tennessee, Knoxville 37996, USA)

([2]School of Mechatronics Engineering, Harbin Institute of Technology, Harbin 150001, China)

Abstract: Microflow driven by AC electrothermal (ACET) effect is explored in order to seek new methods for pumping electrolytes with high conductivity fluid (more than 0.02 S/m) at microscale. Based on the ACET theory, a physical model for particle trapping is established by a set of electrostatics, heat transfer and fluid dynamic equations. Further, fluid velocity fields are predicted using the software FEMLAB. Experiments are performed which verify the numerical results. The experimental results show that with appropriate electrode design, ACET effect can work on fluids with conductivity up to 1.53 S/m and trap particles at a low voltage. ACET devices can be readily integrated on chip into a microsystem. This offers insight into designing ACET lab-chips.

Key words: AC electrokinetics; particle trap; electrothermal effect; numerical simulation

Microfluidic electrokinetics (EK) is gaining popularity as an actuation mechanism for lab-on-a-chip, owing to its simple implementation and reliability from no moving parts. EK can be applied with DC or AC electric sources. DC EK has a long history of development, being investigated and applied extensively[1]. However, DC EK suffers from high voltage operation (several kV) and consequently excessive electrochemical reactions and electrolysis at the electrodes. In the past few years, AC EK has received increasing research interest as it has demonstrated great potential for microfluidic actuation. AC EK has many attractive features. The nonlinear nature of AC EK produces higher transport efficiency than DC EK. AC EK also minimizes undesirable by-products of electrochemical reactions that are unavoidable with DC excitation. Fluid or particle motion generated by AC EK is local, so complex flow patterns can be generated by addressing electrodes individually. This property also makes it possible to manipulate and characterize a single cell or particle. AC electrokinetic devices usually require microscale electrodes and structures, which can now be easily fabricated with good precision by micro technologies such as photolithography and laser micro-machining. All the above factors have greatly motivated the development of AC EK.

AC EK mainly includes dielectro-phoresis (DEP)[2–5], AC electroosmosis (ACEO)[6–9], and AC electrothermal (ACET)[10–12] effect. Both DEP and ACEO have been explored for microfluidic functions, such as concentrating particle and pumping. As for ACET, so far only one application has been reported to enhance the diffusion process in a microfluidic device[12]. This paper reports a particle trap for nanoparticles in conductive media with no external actuation other than an electric field. The device consists of two electrode plates that face each other in parallel at 500 μm separation, which enables handling of a larger fluid volume than other reported configurations[12].

ACET arises from non-uniform electric fields and temperature gradients in the fluids, which produces space charges that move under the influence of electric fields and hence induce microflows. Higher conductivity leads to higher fluid velocity due to increased heat generation and temperature gradients, which is a salient feature setting ACET apart from ACEO. There are several reports on ACEO particle traps. However, ACEO depends on the electric double layer formed at the electrode/electrolyte interface. Higher conductivity compresses the thickness of the double layer, rendering electro-osmosis ineffective. Therefore, ACEO is mainly applicable to fluids with conductivity lower than 0.02 S/m[13].

ACET also has advantages over DEP for concentrating particles. DEP is based on the polarization of particles in a non-uniform electric field and can be used for particle trapping and separation. The efficiency of DEP, or the DEP force, scales with the particle volume, which makes DEP unfavorable when handling

Received 2007-04-26.

Foundation items: US National Science Foundation (No. ECS-0448896), Tennessee Science Alliance Award.

Biographies: Lian Meng (1981—), male, graduate, mlian@utk.edu; Jiang Hongyuan(1960—), male, doctor, professor, jhy_hit@sina.com.

submicron particles, while ACET uses fluid flows to convect particles to certain locations, hence no dependence on particle sizes. Moreover, DEP decreases much faster than ACET with respect to the distance from the electrode (approximately $1/r^3$ for DEP and $1/r$ for ACET). Therefore, ACET is more preferable than DEP and ACEO for bio-fluid and particle manipulation.

1 AC Electrothermal Effect

AC electrothermal effect refers to fluid motion induced by the interaction between temperature gradients in the fluid and electric fields applied over fluids. Electric current passing through the medium generates heat according to the energy balance equation[10-11]:

$$k\nabla^2 T + \frac{1}{2}\langle \sigma E^2 \rangle = 0 \tag{1}$$

where T is the temperature; E is the electric field; k and σ are thermal and electrical conductivities, respectively. With non-uniform electric fields, this heating process produces gradients in local conductivity and permittivity by $\nabla\varepsilon = \left(\frac{\partial\varepsilon}{\partial T}\right)\nabla T$ and $\nabla\sigma = \left(\frac{\partial\sigma}{\partial T}\right)\nabla T$. Further, $\nabla\sigma$ and $\nabla\varepsilon$ generate mobile space charges, ρ_e, in the fluid bulk, by $\rho_e = \nabla(\varepsilon E) = \nabla\varepsilon E + \varepsilon\nabla E$ and $\frac{\partial\rho_e}{\partial t} + \nabla(\sigma E) = 0$ with $\frac{\partial}{\partial t} = \mathrm{i}\omega$ in AC fields. The electric field will impose a force on the induced space charges ρ_e.

$$F_{et} = \rho_e E - \frac{1}{2}|E|^2\nabla\varepsilon \tag{2}$$

The first term in Eq. (2) is the Coulomb force and the second term is the dielectric force. The time averaged force is

$$\langle F_{et}\rangle = -\frac{1}{2}\left(\frac{\nabla\sigma}{\sigma} - \frac{\nabla\varepsilon}{\varepsilon}\right)\frac{\varepsilon|E|^2}{1+(\omega\tau)^2} - \frac{1}{4}\nabla\varepsilon|E|^2 \tag{3}$$

where σ and ε are the electrical conductivity and permittivity of the medium, $\tau = \varepsilon/\sigma$ is its charge relaxation time, and ω is the radian frequency.

For aqueous media at 293 K, $\frac{1}{\varepsilon}\frac{\partial\varepsilon}{\partial T} = -0.004$ and $\frac{1}{\sigma}\frac{\partial\sigma}{\partial T} = 0.02$, Eq. (3) can be calculated to be

$$\langle F_{et}\rangle = -0.012\nabla T\frac{\varepsilon|E|^2}{1+(\omega\tau)^2} + 0.001\nabla T|E|^2 \tag{4}$$

Interesting to note, according to Eqs. (3) and (4), ACET force has no obvious dependency on fluid conductivity. It is because the conductivity dependency is manifested through ∇T. For internally induced ∇T, i. e. from electric currents passing through the fluid, ACET force depends on fluid conductivity according to Eq. (1).

From the discussion above, it can be deduced that the fluid body force follows the directions of the electric field and is proportional to the temperature gradient ∇T. Then the fluid velocity is determined by the Navier-Stokes equation[12],

$$\rho\frac{\partial u}{\partial t} - \eta\nabla^2 u + \rho(\nabla u)u + \nabla P = F_{et} \tag{5}$$

where ρ is the fluid density, η is the dynamic viscosity of the fluid, P is the external pressure and u is the velocity of the fluid. This equation is used later in numerical simulations to obtain the fluid flow fields in our ACET devices. For steady-state fluid motion and without external pressure, Eq. (5) is reduced to $-\eta\nabla^2 u = F_{et}$.

The discussion above shows that the electrothermal force can introduce the fluid motion, and particles are dragged by the fluid viscosity. On the other hand, forces that function on the particle are also able to drive the fluid through viscous drag. In microfluidics structure with particle size at the order of 1 μm, the DEP force cannot be neglected. The DEP mechanism stems from the particle polarization within the electrolyte. Depending on the differences between particle and fluid dielectric properties, two types of DEP forces are formed. When the particle dielectric properties (here we use complex permittivity which is defined as $\varepsilon_p^* = \varepsilon_p - \mathrm{i}\frac{\sigma_p}{\omega}$) are greater than the surrounding fluid, the induced charges at the particle outer surface will dominate and, hence, cause the electric field line to bend towards the particle. When inhomogeneities exist in the electric field, the difference of the Coulomb force acting on the particle dipole leads to the net particle motion towards the field maxima, which is referred to as positive DEP. The converse happens where the particle polarizability is less than that of the electrolyte and negative DEP attracts particles into the electric field minimums.

For particles with radius r suspending in solution with a permittivity of ε_f, the representation of the DEP force magnitude is given by

$$F = 2\pi\varepsilon_f r^3 \mathrm{Re}(f_{CM})\nabla E_{RMS}^2 \tag{6}$$

where f_{CM} is the Clausius-Mossotti factor which reflects the magnitude and direction of the field-induced dipole, given by

$$f_{CM} = \left(\frac{\tilde{\varepsilon}_p - \tilde{\varepsilon}_m}{\tilde{\varepsilon}_p + 2\tilde{\varepsilon}_m}\right) \tag{7}$$

The subscripts p and m stand for particle and medium, respectively; $\tilde{\varepsilon}_p$, $\tilde{\varepsilon}_m$ are the complex permittivities of the particle and the medium; and $\tilde{\varepsilon}_{p,m} = \varepsilon_{p,m} -$

i $\frac{\sigma_{p,m}}{\omega}$. A spherical particle experiencing DEP will exhibit a velocity as

$$\langle u_{DEP} \rangle = \frac{r^2 \varepsilon_m}{6\eta} \mathrm{Re}\left(\frac{\tilde{\varepsilon}_p - \tilde{\varepsilon}_m}{\tilde{\varepsilon}_p + 2\tilde{\varepsilon}_m} \right) \nabla |E|^2 = \frac{r^2 \varepsilon_m}{6\eta} \mathrm{Re}(f_{CM}) \nabla |E|^2 \quad (8)$$

The magnitude of DEP velocity is analyzed to determine its importance in nanoparticle trapping.

Several steps are involved in the numerical simulation when using the above equations to obtain a fluidic field profile. The first step is to use Laplace's equation $\nabla^2 V = 0$ to derive the electric field distribution in the fluidic chamber. The resulting electric field distribution is used to calculate the temperature field according to the energy equation, i. e. Eq. (2). Then the fluid body force in the chamber is calculated using the temperature gradient and the electric field distribution from the first two steps. Finally, the fluid flow field is obtained by the Navier-Stokes equation, i. e. Eq. (5).

2 Parallel Plate Particle Trap

Our ACET particle trap consists of a pair of parallel plate electrodes as shown in Fig. 1. The bottom electrode is shorter than the top one in order to create a non-uniform electric field, which in turn induces a non-uniform temperature field and, further, a fluidic velocity field. Microflows convey particles in the bulk solution to the shorter electrode and deposit them in its center, increasing particle count at that location.

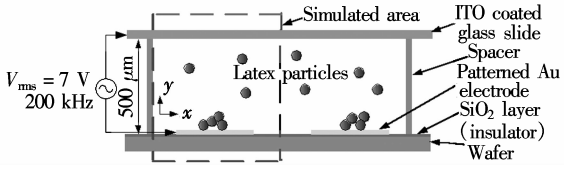

Fig. 1 Schematic of microfluidic chamber

2.1 Numerical simulation

Our ACET trap is simulated using comsol multiphysics (FEMLAB) package. The geometry used in the simulation is given in Fig. 2.

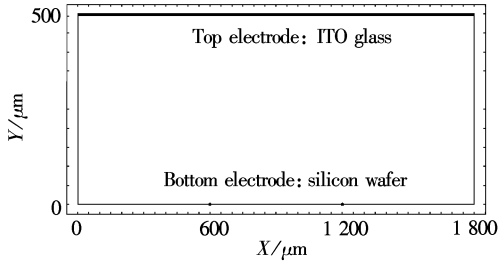

Fig. 2 2-D simulation model

Three sets of boundary conditions are applied to the model, and periodic boundary conditions are applied to the side boundaries so that the effects of adjacent traps are considered. For electric analysis, the bottom electrode is set at 7 V, and the top electrode is grounded. Other parts of the bottom boundary are set as insulators for the electric field. For thermal analysis, the top and bottom electrodes are set at a fixed temperature (e. g. room temperature), acting as heat sinks. For fluid analysis, every boundary is defined as non-slip in order to simulate the sealed chamber situation.

According to Eq. (4), ACET force is a function of the temperature gradient and the electric field. The electric field strength ($E = -\nabla V$) is found to be highest around the edge of the bottom electrode, as shown in Fig. 3(a) and the temperature gradients are also highest near the electrodes (as shown in Fig. 3(b)). Hence the highest fluid velocity is expected to be close to the electrodes, and flowing inward from the edges of the shorter electrodes.

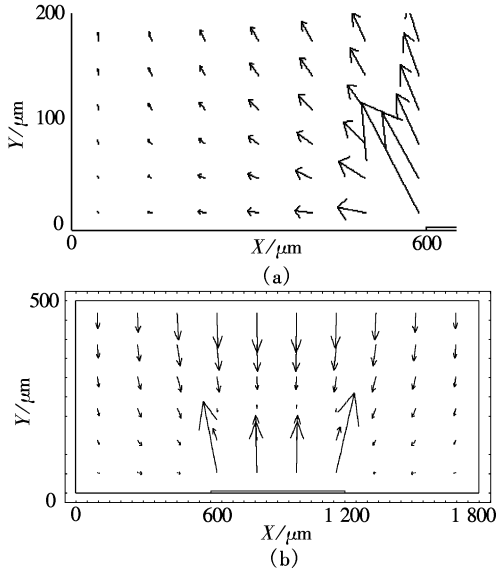

Fig. 3 The electric field strength and temperature gradient. (a) Electric field distribution maximizes at the electrode edge; (b) Temperature gradient

The simulated fluid field is shown in Fig. 4(a), in which the arrow length indicates fluid velocity. Two counter-rotating vortices are produced above the bottom electrode. The flow direction is upwards in the middle and downwards at the sides. The global velocity maximum is seen above the edge of the bottom electrode, where the electrical field strength is at the highest. Flow velocity decreases along the electrode inwards until it becomes zero at the middle. Fluid motions in the middle of the bottom boundary are cancelled out by flows in opposite directions and consequently produce stagnation. It is expected that micro/nano particles be deposited in that area.

To illustrate the relative importance of DEP to

ACET, the DEP velocity profile is shown in Fig. 4(b), calculated by Eq. (8). With the conditions corresponding to the experiments, for 500 μm particles, the DEP velocity has a maximum of 5 μm/s, seen at the bottom electrode edges, and it attenuates quickly when particles are more distant from the edges (shown by the lengths of the arrows). On the other hand, ACET is predicted to have a peak velocity of 57 μm/s. It can be concluded that the electrothermal force is the dominating factor accounting for the fluid motion.

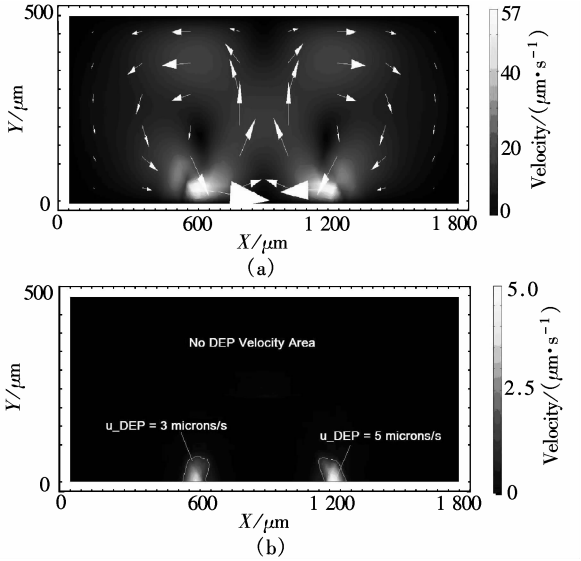

Fig. 4 Simulations of electrothermal and DEP velocity. (a) Simulated electrothermal velocity; (b) Simulated DEP velocity

2.2 Experiments

The parallel particle trap uses a silicon wafer with a patterned Au layer as the bottom electrode (see Fig. 5 (a)) and an indium-tin oxide (ITO) glass slide as the top electrode. A 500-μm-thick spacer (PC8R-0.5, Grace Bio-Labs, Inc.) is put between the electrodes to form a microfluidic chamber, as shown in Fig. 5(b). A NaCl solution (σ = 0.224 S/m) is adopted as the working fluid, in which 500 μm fluorescent particles (molecular probes) are suspended for the purpose of tracking fluid flow. Particle motions are monitored and captured using a Nikon eclipse LV100 microscope and a CCD camera in real time. The images are processed by Image Pro 3 DS (www.mediacy.com. Cybernetics Inc) to extract particle velocity. The electric signal is generated by an Agilent 33220A function generator (Agilent Technology, CO) and then amplified (Model #: 354-1-50, Heico Company) to reach a desired voltage level for electrothermal experiments. Voltages of 4 to 32 V peak to peak at 200 kHz are used in the experiments.

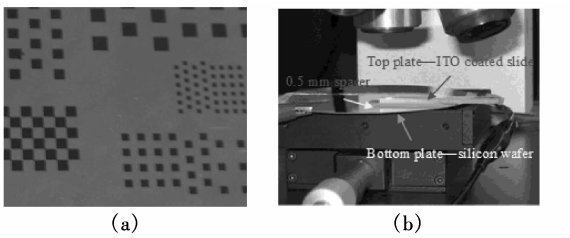

Fig. 5 Experimental equipment. (a) Various electrode patterns on a silicon wafer; (b) Experimental setup

When an AC signal (e.g. V_{pp} = 12 V, 200 kHz) is applied, particles start to make fast circular movements. At the wafer surface, the particles move from the edge of the conductive area towards the center. When the focal plane of the microscope is elevated to be above the wafer (approximately 80 μm), the flow directions are reversed. So it is certain that the fluid is moving in vortices.

Figs. 6(a) and (b) compare the appearance of the wafer surface before and 5 min after a voltage is applied. The accumulation is mostly completed after a few minutes when a large proportion of particles becomes immobilized. As in the simulation, particles are trapped to the centers of the electrodes and, therefore, form the cell-like shapes as shown in Fig. 6(b). Particles also form smaller clusters at the centers of nonconductive regions (shown black in the figure). This is attributed to the symmetry of electrode design where influences of electric fields at those locations are cancelled out.

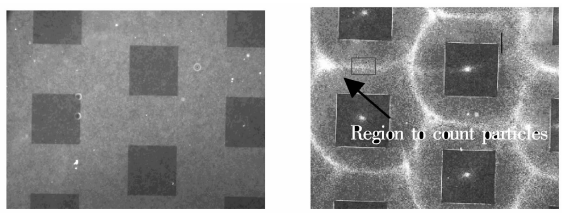

Fig. 6 Electrode surface. (a) Before AC signals being applied to generate convection and to trap particles; (b) After AC signals being applied to generate convection and to trap particles

The trapping effect is quantified in our experiments. Fig. 7 shows the number of particles that are trapped in a designated rectangular area of 360 μm × 225 μm, of which the location is indicated in Fig. 6

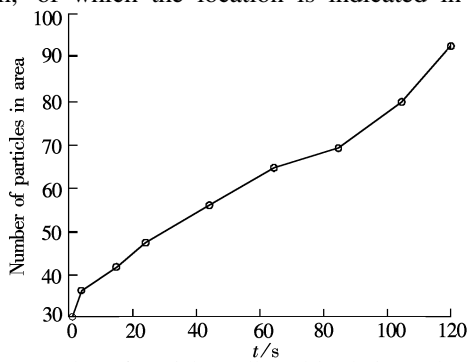

Fig. 7 Number of particles collected in designated area as a function of time

(b). The particle concentration of the experimental solution is 6×10^5 counts/mm^3. At the beginning of the experiment, an initial value of 30 particles in that area is representative of this concentration. The number of trapped particles versus time shows a linear relationship with a positive slope of the trapping ratio at about 0.5 particles/s.

3 Discussion

Theoretically, ACET velocity is expected to follow a quartic relationship with respect to applied voltage. So the voltage dependency of fluid velocity is experimentally studied by varying the applied voltage from 12 to 32 V peak to peak at 200 kHz. For each voltage setting, the four highest particle velocities are chosen to represent the group. To compare theoretical prediction with experimental measurements, regression lines of fitting polynomial $U = cV^4$ is plotted in Fig. 8, where U is the electrothermal velocity; V is the applied voltage; c is a constant associated with conductivity, permittivity and other variables. Fig. 8(a) is the median velocity and Fig. 8 (b) is the maximum velocity from different frames of each selected particle. Experimental data analyzed by JMP 6.0 (SAS Institute, www.jmp.com, NC) show that 78.65% and 77.4% of the velocity data points are explained by the quartic model. It should be noted that ACEO can also be responsible for generating a similar fluid flow pattern[14]. However, since ACEO flow has a quadratic voltage dependence, the above corroborates that ACET is responsible for the fluid motion.

Natural convection, or buoyancy, also has the potential to introduce a similar fluid vortex for the parallel trapping device. Different from the AC electrothermal effect which arises from a temperature gradient, the buoyancy force depends on the temperature rise, which causes the fluid to move from a high temperature region to a low temperature area. The buoyancy generated within the fluidic chamber is produced by the heating process. Its magnitude is equal to the weight of fluid being displaced and can be represented as $f_g = \Delta\rho_m g = \Delta T g \partial\rho_m / \partial T$. The bulk temperature rise in the experimental condition is about 1.73 K, and $\frac{1}{\rho_m}\frac{\partial\rho_m}{\partial T} \approx 10^{-4}$/K. Hence, we can calculate the magnitude of the buoyancy force by $f_g \approx 0.0017$ N/m^3, while the maximum of the electrothermal force is approximately 60.6255 N/m^3, about four orders of magnitude difference. So the effects of buoyancy are negligible compared with those of the electrical forces.

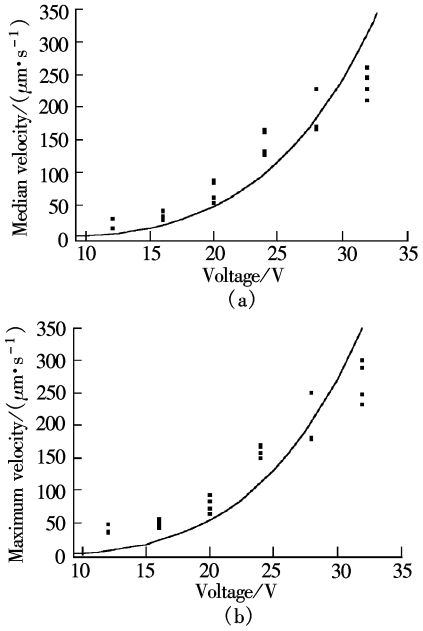

Fig. 8 ACET velocity. (a) Median velocity; (b) Maximum velocity

Not only will particles experience external forces to move from fluid viscosity, but also experience forces such as Brownian motion, gravity due to the difference in mass density between the fluid and the particle, and the influence of electric fields, i.e. DEP. The particle force will induce particle motion, which will be superimposed onto the fluid motion induced by ACET. So it is relevant here to discuss the magnitudes of the particle forces and their contributions in particle trapping.

The particle displacement due to Brownian motion has a zero mean and a standard deviation of $\Delta = \sqrt{\frac{k_B T}{3\pi r\eta}t}$ approximately, where t is the period of operation. For the 500 μm particles that are used in our parallel plate experiment, the standard deviation Δ of particle displacement in one second due to Brownian motion is calculated to be about 25 μm. Over time, the net distance a particle travelling under the influence of Brownian motion will be cancelled out to be zero. The magnitude of the gravitational velocity is $u_g = \frac{2}{9}\frac{r^2\Delta\rho}{\eta}g$, where g is the gravitational acceleration and $\Delta\rho$ is the density difference between particles and fluid. The particles have a mass density of 1.025 g/cm^3, very close to that of water. From the equation above, it is calculated that particle velocity due to gravity is approximately 0.1 μm/s. At such a speed, it would take about 80 h for the gravity to pull the suspended particles from the center of the chamber onto the solid surface. So we can ignore the gravity impact on the particle deposition process.

From both the simulation (see Fig. 4) and the experiments, it can be seen that the DEP force is dominant when particles are close to the field maxima, i.e. the electrode edges in our device. In Fig. 5(b), the

electrode edges are illuminated by the aggregations of fluorescent particles after applying voltage, though to a much weaker degree than in the central parts of the electrodes. The impact of DEP effect is greatly reduced to those located further away from the edge. So it is safe to conclude that the particle aggregation along the centerlines of the electrodes results from the ACET fluid motion.

4 Conclusion

This paper presents a new AC electrothermal device to achieve microfluidic functions, and particle trapping for fluids at conductivity of interest to biochemical analysis. Preliminary experiments of ACET device are successful. As theoretically predicted, fluid velocity scales to the fourth power of applied voltage, and it increases with fluid conductivity. Effective particle and fluid manipulation are demonstrated. Improved performance of ACET devices is expected with optimized design. The advance with ACET devices will greatly expand the application scope of electrokinetics in microfluidic chips.

Acknowledgements The authors thank Professor Nazmul Islam of Northern Arizona University for micro-fabrication of the nanoparticle traps.

References

[1] Thormann W, Lurie I S, McCord B, et al. Advances of capillary electrophoresis in clinical and forensic analysis [J]. *Electrophoresis*, 2001, **22**(19): 4216 − 4243.

[2] Pohl H A. *Dielectrophoresis* [M]. Cambridge: Cambridge University Press, 1995: 40 − 55.

[3] Pethig R. *Application of AC electrical fields to the manipulation and characterization of cells in automation in biotechnology* [M]. Elsevier, 1991: 159 − 185.

[4] Ramos A, Morgan H, Green N G, et al. The role of electrodrodynamic forces in the dielectro-phoretic manipulation and separation of particles[J]. *J Electrostatics*, 1999, **47**(1): 71 − 81.

[5] Gascoyne P R C, Vykoukal J V. Dielectrophoresis-based sample handling in general-purpose programmable diagnostic instruments [J]. *Proceedings of the IEEE*, 2004, **92**(1): 22 − 42.

[6] Green N G, Ramos A, Gonzalez A, et al. Fluid flow induced by nonuniform ac electric fields in electrolytes on microelectrodes: experimental measurements [J]. *Physical Review E*, 2000, **61**(4): 4019 − 4028.

[7] Green N G, Ramos A, Gonzalez A, et al. Fluid flow induced by nonuniform ac electric fields in electrolytes on microelectrodes: observation of streamlines and numerical simulation [J]. *Physical Review E*, 2002, **66**(2): 026305.

[8] Wu J. Electrokinetic microfluidics for on-chip bioparticle processing [J]. *IEEE Trans Nanotech*, 2006, **5**(2): 84 − 89.

[9] Wu J, Islam N, Lian M. High sensitivity particle detection by biased AC electro-osmotic trapping on cantilever[C]// *The* 19*th IEEE Intl Conf on Micro Electro Mechanical Systems* (*MEMS* 2006). Istanbul, Turkey, 2006: 566 − 569.

[10] Ramos A, Morgan H, Green N G, et al. AC electrokinetics: a review of forces in microelectrode structures [J]. *J Phys D*: *Appl Phys*, 1998, **31**(9): 2338 − 2353.

[11] Green N G, Ramos A, Gonzalez A, et al. Electrothermally induced fluid flow on microelectrodes [J]. *J Electrostat*, 2001, **53**(2): 71 − 87.

[12] Sigurdson M, Wang D Z, Meinhart C D. Electrothermal stirring for heterogeneous immunoassays [J]. *Lab on a Chip*, 2005, **5**(12): 1366 − 1373.

[13] Studer V, Pepin A, Chen Y, et al. An integrated AC electrokinetic pump in a microfluidic loop for fast tunable flow control[J]. *Analyst*, 2004, **129**(10): 944 − 949.

[14] Lian M, Islam N, Wu J. Particle line assembly/patterning by microfluidic AC electroosmosis [J]. *J Phys*: *Conf Series*, 2006, **34**(10): 589 − 594.

交流电热效应操控纳米粒子在芯片实验室中的应用

连 萌[1] 吴 杰[1] 姜洪源[2] 杨胡坤[2]

([1] 田纳西大学电子计算机工程系,美国 诺克斯维尔 37996)

([2] 哈尔滨工业大学机电工程学院,哈尔滨 150001)

摘要: 为寻求一种驱动电导率(大于 0.02 S/m)溶液的新方法,探讨了利用交流电热效应驱动高电导率微流体. 根据交流电热效应理论,建立了交流电热粒子诱捕物理模型,利用仿真软件 FEMLAB 对其进行仿真分析研究,并通过实验对其进行验证. 实验结果表明:利用特定的微电极芯片结构和交流电热效应,能驱动流体电导率高达 1.53 S/m 的微流体,实现了在低电势下的粒子诱捕. 利用交流电热效应驱动微流体,不仅能够实现对微粒的诱捕,而且输入信号电势低,受微流体影响小,容易与芯片集成. 研究结果为设计交流电热效应芯片实验室提供了参考依据.

关键词: 交流电热;粒子诱捕;电热效应;数值仿真

中图分类号: O442